ACS APPLIED MATERIALS & INTERFACES

Research Article

www.acsami.org

Understanding the Role of Vanadium in Enhancing the Low-Temperature Hydrogenation Kinetics of an Mg Thin Film

Shiyou Zheng,[†,‡] Zhi-Peng Li,[†] and Leonid A. Bendersky*[,†]

[†]Material Measurement Laboratory, National Institute of Standards and Technology, Gaithersburg, Maryland 20899, United States

[‡]Department of Chemical and Biomolecular Engineering, University of Maryland, College Park, Maryland 20742, United States

ABSTRACT: $Mg_{100-x}V_x$ (x = 0 to 15) thin films capped with Pd were prepared by electron beam codeposition and studied for their hydrogenation/dehydrogenation kinetics and cycling properties at 140 °C under hydrogenation pressures of 0.1 MPa. It has been found that the $Mg_{100-x}V_x$ thin films show significantly higher reversible hydrogen-storage capacity and faster kinetics in comparison with a pure Mg thin film; for instance, the maximum hydrogen absorption (3.7% mass fraction hydrogen) can be obtained in the fifth cycle for $Mg_{90}V_{10}$ in less than 5 min. The addition of V clearly plays a favorable role in improving the reversible hydrogen-storage capacity of an Mg film; however, with increasing hydrogenation/dehydrogenation cycles the hydrogen-storage capacity gradually deteriorates. To explore the origin of the effect of V on the improved hydrogenation of an Mg thin film, in this work we focused on studying the structural variations of the $Mg_{90}V_{10}$ thin film before and after hydrogenation at different stages of cycling; the films were investigated by X-ray diffraction as well as scanning and transmission electron microscopy. We concluded that (1) early in the absorption/desorption cycling the as-deposited structure of percolating layers of nanocrystalline V throughout a Mg matrix is preserved; (2) the percolating V layers envelope fine Mg grains and act as (a) dispersers that isolate small Mg grains, (b) fast diffusers of hydrogen, and (c) hydrogen catalysts at the Mg/V interface to form MgH_2; and (3) with progressive cycling, the continuous layers of V aggregate to spherical nanoparticles, which interrupts the continuity of fast hydrogen diffusion through V.

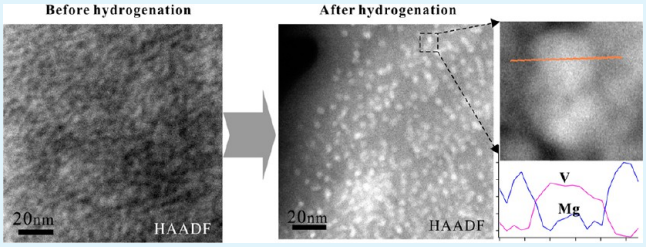

KEYWORDS: *thin film, Mg−V, hydrogen storage, TEM*

1. INTRODUCTION

Using hydrogen as an emission-free fuel for automotive technologies requires the high-capacity storage of hydrogen operating at temperatures below 150 °C and pressures ranging from near ambient to about 10 MPa; another essential component is the necessity of fast kinetics during charging/discharging.[1] These and other requirements favor storage on the basis of solid-state materials rather than on compressed or liquid hydrogen, which requires high pressures (70 MPa) or low condensation temperatures (−253 °C), respectively. In spite of extensive research, no known materials can immediately fulfill these requirements; significant efforts went into engineering advanced materials with optimal thermodynamic and kinetic properties. Mg-based hydrides have attracted great attention in the development of solid-state hydrogen-storage systems because of the high gravimetric hydrogen capacity of its hydride, MgH_2, and low cost of Mg. However, from a practical point view, they are severely hindered by their high thermodynamic stability and sluggish kinetics, which lead to excessively high operating temperatures $T \geq 400$ °C for bulk materials.[2,3] Most studies to improve Mg have been focused on the modification of thermodynamic and hydrogen kinetics properties by ball milling refinement, alloying Mg with different constituencies, or adding catalysts.[4−6] It has been found that Mg has shown significantly accelerated kinetics in bulk systems when alloyed with transition-metal (TM) elements such as Ti, Cr, V, Sc, Fe, and so forth.[7−10] To understand the fundamental origins of the effect that TMs have on the improvement of the hydrogen-storage properties of Mg, a significant number of publications were dedicated to study Mg-based thin films because a thin-film structure and composition presumably can be better controlled than powders or bulks.[11−15] Mg−V alloys have been studied in bulk systems and showed accelerated kinetics relative to Mg. Along with many other TMs, V is immiscible with Mg, which was identified in our previous studies of Mg−Fe as a major feature affecting hydrogenation improvement. However, hydrogenation and dehydrogenation in the Mg−V thin-film systems have received little attention; for example, Mitlin et al. studied ternary Mg−Cr−V films and found a significant improvement with respect to the pure Mg film at 200 °C that was, however, accompanied with a high density of surface cracks after prolonged cycling.[16] In our previous investigation of codeposited Mg−Fe thin films, we have demonstrated that the hydrogen uptake and release kinetics at 140 °C are remarkably enhanced even with a small amount of Fe; surfaces of the films remained almost intact after 10 cycles of hydrogenation/dehydrogenation.[17,18] To extend what has been learned for the Mg−Fe thin films to other Mg−

Received: March 24, 2013
Accepted: July 19, 2013
Published: July 19, 2013

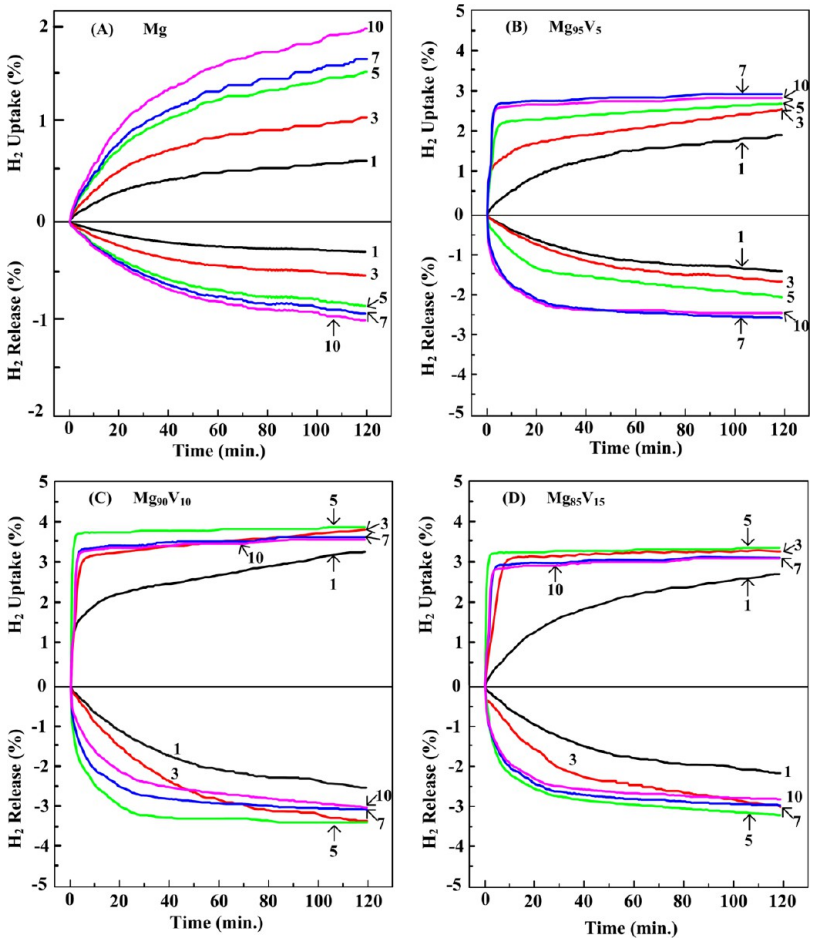

Figure 1. Hydrogen absorption and desorption kinetics curves during different cycles for Mg–V thin films: (A) Mg, (B) $Mg_{95}V_5$, (C) $Mg_{90}V_{10}$, and (D) $Mg_{85}V_{15}$.

TM systems, $Mg_{100-x}V_x$ (x = 0 to 15) thin films capped with Pd were herein prepared by electron beam codeposition and studied for their hydrogenation/dehydrogenation kinetics and cycling properties under similar moderate conditions. $Mg_{90}V_{10}$ was chosen as the model system to explore the origins of the effect of V on the hydrogen storage of an Mg thin film. The structures of the thin films before and after hydrogenation during different cycles were investigated by X-ray diffraction (XRD), scanning electron microscopy, (SEM) and transmission electron microscopy (TEM).

2. EXPERIMENTAL PROCEDURES

Thin Films Preparation. $Mg_{100-x}V_x$ (x = 0, 5, 10, and 15) thin films with a thickness of 1 μm were deposited on c-Al_2O_3 substrates under ultra-high vacuum by electron beam coevaporation. All films were deposited without heating and subsequently capped with a 6 nm thick Pd layer to not only prevent oxidization during handling but also mainly to facilitate the dissociation of hydrogen molecules. The film thickness and composition were controlled in situ via crystal monitors. Compositions of the as-deposited thin films were confirmed to be very close to the designed compositions by X-ray energy dispersive spectroscopy (EDS) measurements. The EDS analysis was performed with a Hitachi S-4700 field emission scanning electron microscope (FE–SEM) with an Oxford INCA EDS system. Pure Mg without V was also deposited under the same conditions for comparison. All deposited samples were transferred to and stored in a glovebox filled with high purity Ar gas with a moisture level less than 0.03 μL/L to prevent oxidation. Hydrogen volumetric loading/unloading was performed in a Sieverts apparatus developed at the National Institute of Standards and Technology (NIST) with a high precision pressure transducer (0.003% FS) over a relatively wide pressure range.[18] All hydrogen absorption measurements were carried out at 140 °C under 0.1 MPa H_2 pressure for 2 h; hydrogen desorption was performed at the same temperature for 2 h by keeping low ambient pressure (10 Pa). Before the next absorption step, to ensure that the charging hydrogen was discharged completely, the samples were evacuated for another 30 min after each desorption step measurement. For all of the samples, at least 10 hydrogen absorption/desorption cycles under the same hydrogen loading/unloading conditions were measured.

SEM images were obtained with a Hitachi S-4700 FE–SEM at 5.0 kV. Crystalline phases in the thin films at different stages of absorption/desorption and cycling were analyzed by X-ray diffraction (XRD) (Rigaku D/max 2400 with Cu Kα radiation). The hydrogenated samples during different cycles were obtained by absorbing hydrogen under the above-mentioned conditions and then cooling to room temperature under the hydrogenation pressure.

Cross-sectional TEM samples of the as-deposited and hydrogenated films were prepared by a water-free polishing procedure and ion milling in a liquid-nitrogen cooled stage in an attempt to preserve the structural features of the films. The TEM samples were examined with a JEM 3010 microscope. High spatial resolution imaging and microanalysis were performed with an FEI Titan 80-300 analytical scanning transmission electron microscope (STEM) operated at 300 kV accelerating voltage and equipped with a Fischione Instruments model 3000 high-angle annular dark-field (HAADF) detector and an EDAX lithium-drifted silicon X-ray energy-dispersive spectrometer (XEDS).

3. RESULTS

3.1. Hydrogen Absorption and Desorption Kinetics. The hydrogen absorption and desorption kinetics curves for the $Mg_{100-x}V_x$ (x = 0, 5, 10, and 15) thin films during the first, third, fifth, seventh, and tenth cycles at 140 °C are compared in Figure 1. The jaggedness of some curves is due to instrumental noise. Figure 1A shows the absorption and desorption behaviors for the pure Mg thin film; the parabolic curves exhibit sluggish kinetics and incomplete hydrogen charging/discharging at 140 °C after 120 min (complete conversion of Mg into MgH_2 should give a 7.6% mass fraction of hydrogen). During the first cycle, the Mg thin film absorbs less than a 0.6% mass fraction of hydrogen and desorbs around a 0.3% mass fraction in 120 min With an increasing number of cycles, both the absorption and desorption have significantly improved; however, even after 10 cycles, only a 1.8% mass fraction of hydrogen can be absorbed and about a 1.0% mass fraction can be desorbed in 120 min. This is far less than the theoretical value of 7.6% mass fraction expected for a fully hydrogenated film, which indicates that only a part of the Mg was transforming to MgH_2 under the experimental conditions. The difference in the amounts of absorbed and desorbed hydrogen during the 120 min cycle indicates the presence of trapped hydrogen; the trapped hydrogen was removed before the next cycle. These features are consistent with the results reported previously.[19]

For the $Mg_{95}V_5$ sample (Figure 1B), there exists an apparent activation period of about five cycles during which the absorption/desorption kinetics is relatively slow, but it is obvious that more hydrogen can be absorbed and desorbed in $Mg_{95}V_5$ than in the pure Mg thin film. During even the first cycle, $Mg_{95}V_5$ can reversibly absorb and desorb 4 times more hydrogen than Mg. After the five-cycle activation, the $Mg_{95}V_5$ film shows extremely fast charge/discharge kinetics and increased capacity: 2.7% mass fraction of hydrogen uptake and 2.2% mass fraction of hydrogen release. The measurements clearly demonstrate that the addition of a small amount of V to Mg significantly accelerates the kinetics of hydrogenation. For the $Mg_{90}V_{10}$ sample (see Figure 1C), the maximum hydrogen absorption and desorption capacities can be obtained in the fifth cycle, that is, a 3.7% mass fraction of hydrogen will be absorbed in less than 5 min and a 3.0% mass fraction of hydrogen will be desorbed in less than 60 min. As the cycling continues, the capacities start to deteriorate to some degree (e.g., about 3.3% absorbed after tenth cycle in comparison to 3.7% after the fifth); however, the shape of the absorption/desorption kinetics curves is almost identical. The cycling absorption and desorption behavior for the $Mg_{85}V_{15}$ films is almost identical to that of the $Mg_{90}V_{10}$ film, with the exception of a slightly lower hydrogen content resulting from the higher density of the higher V content films; a further increase in V concentration does not contribute to better reversible hydrogen-storage properties. Again, similar to $Mg_{95}V_5$ and $Mg_{90}V_{10}$, the hydrogen capacities slightly degrade with continued cycling.

Mg films codeposited with V (up to 15% atom fraction) show a dramatic improvement in their kinetics and reversibility of hydrogenation at low temperatures in comparison to pure Mg. There is an activation period of about five cycles, after which the hydrogenation and desorption rates dramatically improve and remain reproducible. With continued cycling, a slight decrease in capacity occurs for all studied compositions. To gain insight into the role of V on the enhancement of the hydrogen-storage properties of Mg−V thin films, we selected $Mg_{90}V_{10}$ to investigate its structural characteristics at different stages of hydrogenation in detail. By considering the very similar hydrogenation behavior of all of the studied compositions, we believe that the conclusions derived for $Mg_{90}V_{10}$ are applicable for all studied films.

3.2. Structural Analysis. *3.2.1. XRD.* XRD patterns of the as-deposited pure Mg, as-deposited $Mg_{90}V_{10}$, and hydrogenated $Mg_{90}V_{10}$ after the first, fifth, and tenth cycle are shown in Figure 2. The pattern of the as-deposited $Mg_{90}V_{10}$ film is almost identical to that of the as-deposited Mg film: both patterns consist of the well-defined (0002) Mg peak at ≈34.5 degrees, the broad (111) Pd peak around 40 degrees, and the (0006) Al_2O_3 peak at 42 degrees from the *c*-cut sapphire substrate.[17] Peaks of the expected bcc-V phase are invisible in the pattern of the as-deposited $Mg_{90}V_{10}$ film. Taking into consideration the very low solubility of V in Mg and the absence of Mg−V intermetallic phases, this observation suggests that V was segregated in either an amorphous or nanocrystalline state; similar XRD results were observed for codeposited Mg−Fe films studied recently.[17,18] After the first hydrogen absorption cycle, the (110) MgH_2 peak appears on the XRD scan along with the Mg (0002) peak in the $Mg_{90}V_{10}$ sample (Figure 2c). In comparison to the as-deposited $Mg_{90}V_{10}$, the intensity of the Mg peak has decreased after hydrogenation; however, it is noticeably lower than that for the hydrogenated Mg film (data not shown). The coexistence of the Mg and MgH_2 phases implies an incomplete transformation during the first cycle, which in turn explains why less hydrogen mass was observed in the hydrogen absorption measurement. With further cycling, one can see that after the fifth cycle (Figure 2d) the Mg peaks have almost vanished, indicating near-full hydrogenation at 140 °C with 0.1 MPa H_2 pressure for 2 h. Upon continued cycling, the XRD patterns of the hydrogenated $Mg_{90}V_{10}$ sample (Figure 2e) remain almost identical to that of the fifth cycling sample, but the weak peak of Mg remains. The presence of the Mg peak suggests that the $Mg_{90}V_{10}$ thin film cannot achieve complete hydrogenation under these moderate conditions. The difference between fifth and tenth cycle is in the reappearance of Mg, which suggests that some structural changes occur. Overall, the interpretation of the XRD results is in agreement with the volumetric measurements.

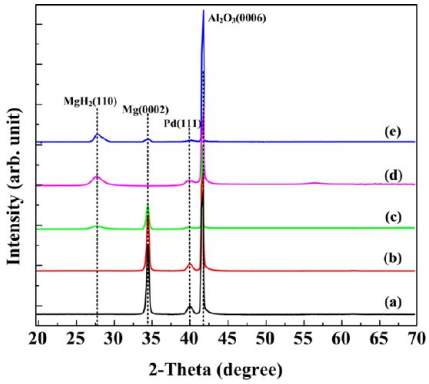

Figure 2. XRD patterns of the as-deposited pure Mg, as-deposited $Mg_{90}V_{10}$, and hydrogenated $Mg_{90}V_{10}$ during different cycles: (a) as-deposited pure Mg, (b) as-deposited $Mg_{90}V_{10}$, (c) hydrogenated $Mg_{90}V_{10}$ during the first cycle, (d) hydrogenated $Mg_{90}V_{10}$ during the fifth cycle, and (e) hydrogenated $Mg_{90}V_{10}$ during the tenth cycle.

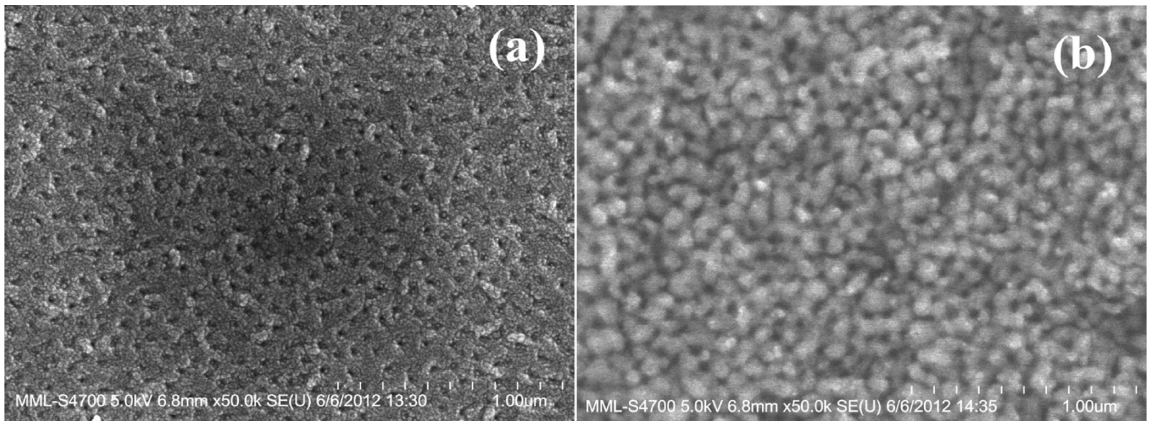

Figure 3. SEM images of the $Mg_{90}V_{10}$ thin film: (a) as-deposited sample and (b) hydrogenated sample in the tenth cycle.

3.2.2. SEM. Surfaces of the as-deposited and 10-cycle hydrogenated $Mg_{90}V_{10}$ film were characterized by SEM (Figure 3a,b). Three features are noted: (i) the surface morphology of the as-deposited $Mg_{90}V_{10}$ film shows that the Pd capping layer is continuously covering the film and consists of small grains (about 10 to 15 nm in diameter) and triple-junction holes are also present (Figure 3a); (ii) a comparison of the hydrogenated and as-deposited films shows that the Pd surface remains practically unchanged after 10 cycles; thus, significant volume expansions accompanying the MgH_2 hydride formation during cycling do not induce a cracking or peeling off of the films; and (iii) hydrogenation-induced grain growth in the Pd layer is also apparent.

3.2.3. TEM. To understand the spatial distribution of V, high-angle annular dark-field (HAADF) imaging operated in scanning transmission electron microscopy (STEM) mode was performed along with TEM. Because of the different scattered angles produced by different elements, the HAADF images reveal different intensities directly related to the atomic number of constituent elements in the material, namely, bright regions should be attributed to the presence of higher atomic number (high-Z) elements, which is V ($Z_V = 23$ and $Z_{Mg} = 12$).

The microstructures of the $Mg_{90}V_{10}$ thin films in the as-deposited and cycled states are shown Figure 4. The as-deposited films are dense and well adhered to the Al_2O_3 substrate, and they show a microstructure of columnar grains (Figure 4a,b). Because of the chemical sensitivity of HAADF imaging, it is quite easy to distinguish different layer structures in the thin-film sample, as denoted in the figures. The structure of the films after being cycled five times did not show noticeable microstructural changes. However, after 10 cycles of hydrogenation (Figure 4c,d), the TEM images show that a network of microcracks has developed, although the films remain intact.

Selected area electron diffraction (SAED) patterns from the as-deposited films (Figure 5a) show spotty diffraction rings, which were indexed as hcp-Mg. In addition, a continuous diffuse ring situated between Mg(01-11) and Mg(10-12) was indexed as (011) of bcc-V. The SAED patterns indicate that the Mg phase is polycrystalline and textured, whereas V appears as nanometer-sized randomly oriented grains. SAED patterns of hydrogenated samples (after 10 cycles) show the presence of diffraction rings corresponding to the MgH_2 phase as well as V and Mg.

High-resolution TEM (HRTEM) and HAADF imaging allowed the observation of the essential microstructural details.

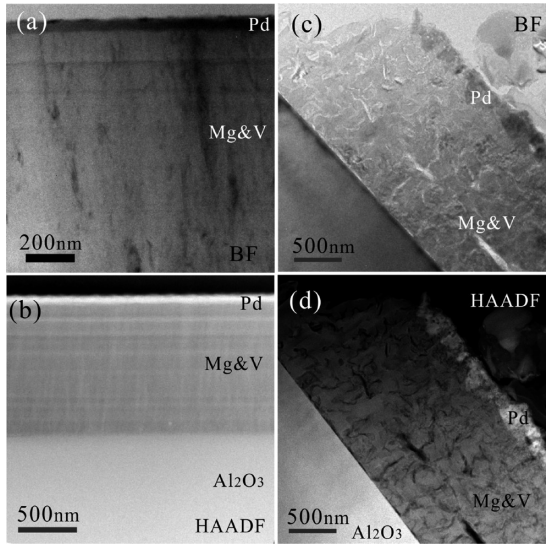

Figure 4. Cross-sectional TEM bright field (BF) and HAADF images of $Mg_{90}V_{10}$ thin films in the as-deposited state (a, b) and after 10 cycles of the H_2 sorption/desorption processes (c, d).

The HRTEM images of the as-deposited $Mg_{90}V_{10}$ thin film (Figure 6a) reveal the presence of nanocrystalline grains that were identified as bcc-V by measuring the lattice fringes. The HAADF image(Figure 6b) shows that V (the brighter regions of the Z contrast) is forming a continuous network that uniformly percolates the Mg film. By combining these two imaging methods, one can conclude that the as-deposited films comprise a microstructure of continuous V layers that envelope small grains of Mg; the structure of the V layers consists of randomly oriented nanosize bcc grains. Figure 6c,d represents a microstructure after cycling; considerable microstructural change in comparison to the as-deposited structure is evident. It can be seen that after five cycles the continuity of the V layers was disrupted into the formation of spherical crystalline V particles (average size ≈4 nm) homogeneously embedded in the Mg matrix. These disconnected V particles are uniformly distributed throughout the film, as seen clearly in the HAADF image of Figure 6d. With further cycling, the spherical nanoparticles are slightly coarsened (Figure 6e,f) and have wider separation.

Figure 7a shows an HRTEM image of a typical spherical nanoparticle observed in the $Mg_{90}V_{10}$ film after 10 sorption cycles. Its crystalline structure is determined from the

dx.doi.org/10.1021/am402450w | ACS Appl. Mater. Interfaces 2013, 5, 6968−6974

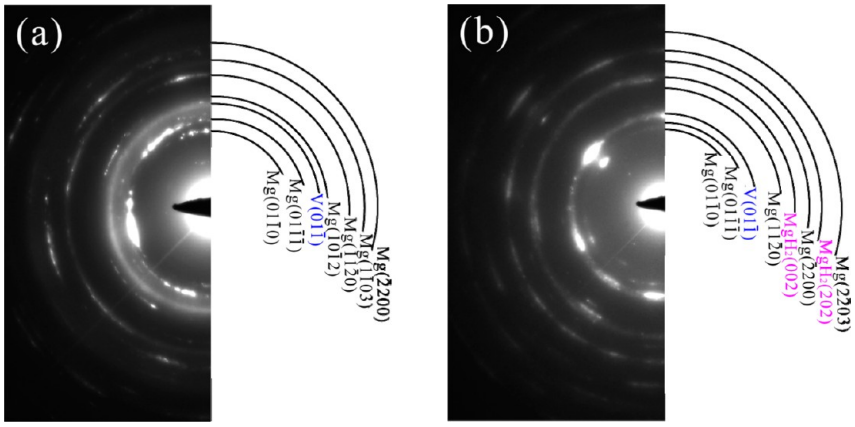

Figure 5. SAED patterns of the $Mg_{90}V_{10}$ thin film before hydrogenation (a) and after 10 cycles of the H_2 sorption processes (b).

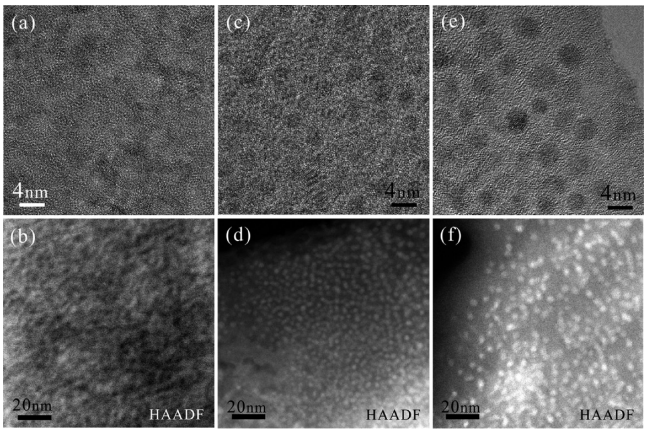

Figure 6. HRTEM observations of $Mg_{90}V_{10}$ thin films (a) before H_2 adsorption, (c) after five cycles and (e) after 10 cycles of the hydrogen sorption processes. The corresponding HAADF images are shown in panels b, d, and f, respectively.

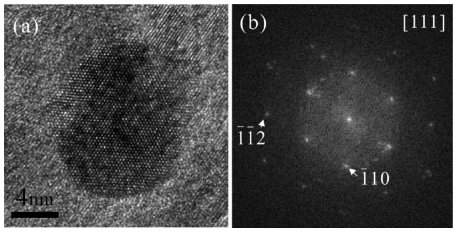

Figure 7. (a) HRTEM of a typical sphere-like nanoparticle embedded in an $Mg_{90}V_{10}$ thin film after 10-cycles of the hydrogen sorption processes. The corresponding FFT result is shown in panel b.

corresponding fast Fourier transform (FFT) (Figure 7b) as the [111] zone axis of bcc-V, which confirms the results of the HAADF imaging. Another confirmation that the particles are bcc-V came from measuring the element distribution around the spherical nanoparticles using line-scan STEM/XEDX analysis, as shown in Figure 8a,b.

4. DISCUSSION

From the experimental results, the following conclusions with regard to the effects of V on hydrogen storage and microstructural properties can be derived: (i) Mg thin films codeposited with V show significantly higher reversible hydrogen-storage capacity and faster kinetics than that of the

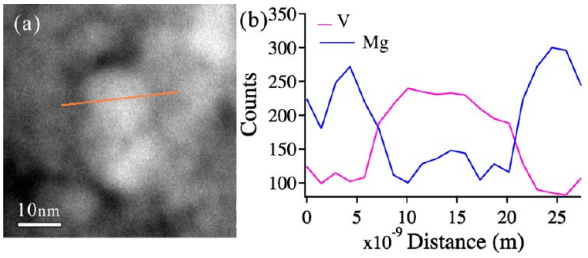

Figure 8. (a) STEM DF image of $Mg_{90}V_{10}$ after 10 cycles of hydrogen sorption. The STEM EDX line scan is conducted across a typical spherical nanoparticle. The corresponding result is shown in panel b.

pure Mg thin film, especially in the early stages of the absorption/desorption cycling; (ii) with increasing hydrogenation/dehydrogenation cycles, some deterioration in the reversible hydrogen-storage capacity is occurring; (iii) as-deposited $Mg_{90}V_{10}$ has a structure of the continuous layers of V percolating the Mg matrix (such structures present in other compositions); and (iv) with prolonged cycling, this layer structure evolves into a homogeneous distribution of isolated spherical particles of V.

The observed effect of V on the low-temperature hydrogenation of Mg films appears to be similar to what was observed in our recent work on the hydrogenation of Mg–Fe films. Similar to Fe, V is immiscible with Mg, has limited solubility, and does not form intermetallic compounds. Thus, during film deposition, the phase separation of V and Mg occurs, and for the combination of deposition temperature, deposition rate, and surface/bulk diffusion of V and Mg that were used, the microstructure with percolation of continuous layers of V throughout an Mg film was synthesized. The formation of the two-phase structure in the undercooled conditions of the film-deposition process helps to refine the structure and disperse Mg; thus, the small grains of Mg can be hydrogen charged/discharged quickly before a critical thickness of growth-limiting MgH_2 is reached.[20]

The role of V in the low-temperature hydrogenation of Mg–V thin-film systems is explained here with the help of schematic drawings given in Figure 9. The microstructure of the films in the as-deposited state, (Figure 9a) and in the early stages of absorption/desorption cycling (Figure 9b) consists of layers of V percolating throughout the Mg film and enveloping small (about 10 nm in diameter) grains of Mg. These V layers act as fast diffusers for hydrogen, through which hydrogen atoms reach Mg grains in the entire film in a short time. The fast

dx.doi.org/10.1021/am402450w | ACS Appl. Mater. Interfaces 2013, 5, 6968–6974

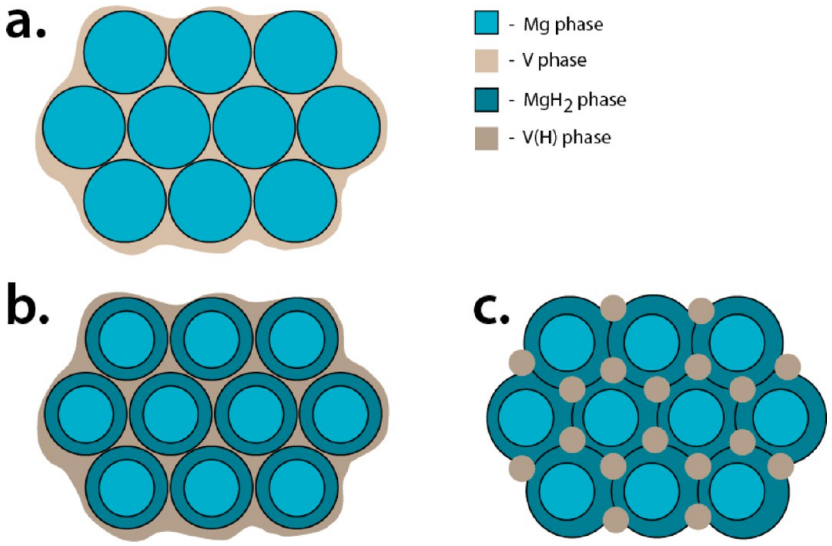

Figure 9. Schematic drawing showing microstructural evolution occurring in Mg–V films during hydrogenation/dehydrogenation cycling. (a) Microstructure of the films after deposition, (b) microstructure at the early stages of absorption/desorption cycling, and (c) microstructure at the late stages of absorption/desorption cycling.

diffusion rate of hydrogen at relatively low temperatures is typical for all bcc transition metals (e.g., bcc-Fe). On the basis of the diffusion coefficient of H in bcc-V at 100 °C, it will take only 1 min for hydrogen to penetrate the entire film.[21] The hydrogen-saturated V layers act as a source of hydrogen to convert the Mg grains that contact V into MgH_2. By considering the small Mg grains, converting an entire 10 nm Mg grain into a hydride phase will take a few seconds (on the basis of the growth rate of MgH_2 measured directly in ref 18). At the same time, V on the Mg/V surface (or rather interface) will also act as a catalyst to promote the nucleation of the hydride.[22] Thus, the continuity of fast hydrogen delivery to small Mg grains is the fundamental reason for the observed highly reversible hydrogen-storage capacity and fast kinetics.

With progressive cycling, the repeating volume changes of Mg ⇔ MgH_2 transformation (about 30%) would result (similar to fatigue phenomena) in the generation of a high density of defects (i.e., dislocations, prismatic loops, and vacancies). The presence of these defects contributes to the enhancement in self-diffusion of both Mg and V; this enhancement promotes the coarsening of Mg grains that aggregate into larger particles. Aggregation of the Mg grains disrupts the continuity of the V layers, and the V layers evolve by diffusion into segregated globular particles (Figure 9c). The interrupted continuity introduces segments of the Mg phase of slower hydrogen diffusion into the hydrogen pass throughout a film. Although a microstructure with V in the form of unconnected particles is still efficient in kinetic improvement for Mg-based thin films, the interrupted diffusion of H via the V phase and the increased size of the Mg grains (up to a micrometer in size) affect adversely both its kinetics and capacity.[23]

5. CONCLUSIONS

The present work demonstrates clearly that the $Mg_{100-x}V_x$ (x = 0 to 15) thin films have significantly higher reversible hydrogen-storage capacity and faster kinetics than the pure Mg thin films under moderate hydrogenation conditions. With continuing hydrogenation/dehydrogenation cycling, a gradual deterioration in the reversible hydrogen storage occurred. On the basis of the microstructural analysis of the as-deposited and hydrogenated $Mg_{90}V_{10}$ in different cycles, we conclude the following: (1) early in the absorption/desorption cycling, V layers percolate, envelope, and disperse Mg grains and thus act as a media supplying fast-diffusing hydrogen throughout the whole film as well as a catalyst to favor the dissociation and reassociation of hydrogen and (2) with progressive cycling, the Mg grains aggregates into larger particles and at the same time the V layers disrupt and aggregate into isolated particles, which leads to less favorable situations for the diffusion of H via the V phase into Mg grains.

AUTHOR INFORMATION

Corresponding Author

*E-mail: leoben@nist.gov. Phone: +1-301-975-6167.

Notes

The authors declare no competing financial interest.

ACKNOWLEDGMENTS

The authors thank Dr. Ke Wang of the Pennsylvania State University (U.S.A.), Dr. Chun Chiu of Natural Resources Canada (Canada), and Mr. Robert Parke and Ms. Sandra Claggett of the National Institute of Standards and Technology (U.S.A.) for their help in the preparation and measurements of the samples. Certain commercial equipment, instruments, and materials are identified in this document. This identification does not imply the recommendation of or endorsement by the National Institute of Standards and Technology nor does it imply that the products identified are necessarily the best available for the purpose.

REFERENCES

(1) Schlapbach, L.; Zuttel, A. *Nature* **2001**, *414*, 353–358.
(2) Reilly, J. J.; Wiswall, R. H. *Inorg. Chem.* **1968**, *7*, 2254–2256.
(3) Grochala, W.; Edwards, P. P. *Chem. Rev.* **2004**, *104*, 1283–1315.
(4) Aizawa, T.; Kuji, T.; Nakano, H. J. *J. Alloys Compd.* **1999**, *291*, 248–253.
(5) Orimo, S.; Fujii, H. *Appl. Phys. A* **2001**, *72*, 167–168.
(6) Liang, G.; Huot, J.; Boily, S.; Van Neste, A.; Schulz, R. J. *J. Alloys Compd.* **1999**, *292*, 247–252.

(7) Baldi, A.; Gremaud, R.; Borsa, D. M.; Balde, C. P.; Van der Eerden, A. M. J.; Kruijtzer, G. L.; Int, J. *Int. J. Hydrogen Energy* **2009**, *34*, 1450−1457.
(8) Zahiri, B.; Amirkhiz, B. S.; Danaie, M.; Mitlin, D. *Appl. Phys. Lett.* **2010**, *96*, 013108-1−013108-3.
(9) Juskenas, R.; Kapocius, V.; Karpaviciene, V. J. *J. Alloys Compd.* **2009**, *467*, 524−527.
(10) Er, S.; de Wijs, G. A.; Brocks, G. *J. Phys. Chem. Lett.* **2010**, *1*, 1982−1986.
(11) Barcelo, S.; Rogers, M.; Grigopoulos, C. P.; Mao, S. S. *Int. J. Hydrogen Energy* **2010**, *35*, 7232−7235.
(12) Remhof, A.; Borgschulte, A. *Chem. Phys. Chem.* **2008**, *9*, 2440−2455.
(13) Ye, S. Y.; Chan, S. L. I.; Ouyang, L. Z.; Zhu, M. *J. Alloys Compd.* **2010**, *504*, 493−497.
(14) Zahiri, B.; Amirkhiz, B. S.; Mitlin, D. *Appl. Phys. Lett.* **2010**, *97*, 083106.
(15) Gremaud, R.; Baldi, A.; Gonzalez-Silveira, M.; Dam, B.; Griessen, R. *Phys. Rev. B* **2008**, *77*, 144204-1−144204-10.
(16) Zahiri, B.; Danaie, M.; Tan, X.; Amirkhiz, B. S.; Botton, G. A.; Mitlin, D. *J. Phys. Chem. C* **2012**, *116*, 3188−3199.
(17) Zheng, S.; Wang, K.; Oleshko, V. P.; Bendersky, L. A. *J. Phys. Chem. C* **2012**, *116*, 21277−21284.
(18) Tan, Z.; Chiu, C.; Heilweil, E. J.; Bendersky, L. A.; Int, J. *Int. J. Hydrogen Energy* **2011**, *36*, 9702−9713.
(19) Zahiri, B.; Harrower, C. T.; Amirkhiz, B. S.; Van Neste, A.; Mitlin, D. *Appl. Phys. Lett.* **2009**, *95*, 103114.
(20) Baldi, A.; Dam, B. *J. Mater. Chem.* **2011**, *21*, 4021−4026.
(21) Luo, J.; Zhou, H.; Liu, Y.; Gui, L.; Jin, S.; Zhang, Y.; Lu, G. *J. Phys.: Condens. Matter* **2011**, *23*, 135501.
(22) Bazzanella, N.; Checchetto, R.; Miotello, A. *J. Nanomater.* **2011**, 865969-1−865969-11.
(23) Zhang, X.; Yang, R.; Qu, J.; Zhao, W.; Xie, L.; Tian, W.; Li, X. *Nanotechnology* **2010**, *21*, 095707.